Science Advances
AAAS

advances.sciencemag.org/cgi/content/full/5/4/eaau4299/DC1

Supplementary Materials for

Urban heat island: Aerodynamics or imperviousness?

Dan Li*, Weilin Liao, Angela J. Rigden, Xiaoping Liu, Dagang Wang, Sergey Malyshev, Elena Shevliakova

*Corresponding author. Email: lidan@bu.edu

Published 3 April 2019, *Sci. Adv.* **5**, eaau4299 (2019)
DOI: 10.1126/sciadv.aau4299

This PDF file includes:

Supplementary Text

Model simulations.

The model used in this study is the Geophysical Fluid Dynamics Laboratory (GFDL) land model LM3 (*20*, *21*), coupled with a newly developed and evaluated urban canopy model (UCM) (*22*, *23*). Within each grid cell, LM3 represents different land-use/land-cover types as a collection of tiles (*20*, *21*). Each tile has its own energy and water balances throughout the vegetation-soil column and its own exchange coefficients with the atmosphere, but the atmosphere only receives the area-averaged fluxes of the grid cell. The land-use/land-cover types in LM3 include natural and secondary vegetation, grassland, pasture, and urban.

The UCM is built on the urban canyon concept and separates the urban land into roof and canyon (*22*). It considers important radiation processes in the urban canyon including sky-view factors, shadow effects, and multiple reflections between walls and ground surfaces. It parameterizes turbulent exchanges between the atmosphere, the canopy air, walls and ground surfaces through a resistance approach. It also incorporates radiative, hydrological and biological processes associated with vegetation within the urban canyon. It solves the surface energy balance equations for different urban facets, including roof, wall, impervious ground, and pervious ground. Evaluation of the UCM using observational eddy-covariance data sets can be found in Ref. *22*.

In this study, the LM3 coupled with the UCM is driven by atmospheric forcing from GFDL earth system model outputs (the GFDL forcing) or gridded datasets based on observations and reanalysis fields (the Sheffield forcing). The GFDL forcing refers to outputs from coupled land-atmosphere-ocean earth system model simulations for the Coupled Model Intercomparison Project Phase 5 (CMIP5) (*28*, *29*), which did not use any UCM in the land component. Specifically, the 3-hourly, 2 by 2.5 degrees ESM2Mb model outputs in the historical period and

under the representative concentration pathway 8.5 are used (*30*). The Sheffield forcing (*31*) refers to the 50-yr (1949-2000), 3-hourly, 1-degree data set, which is based on a combination of observational and reanalysis data. The forcing variables for all experiments include downward shortwave radiation, downward longwave radiation, air temperature, specific humidity, pressure, wind speed, and precipitation.

Using the GFDL forcing, we conduct long-term simulations (from 1700 to 2100) over North America (20°N – 55°N, 130°W – 60°W). Using the Sheffield forcing, we also conduct the simulations from 1700 to 2000 and we apply the first 30-yr forcing to the period of 1700-1948 in order to spin-up the model. Given the difference between the resolutions of the two forcing data sets, we use a grid resolution of 50 km for a consistent comparison. We focus on the UHIs in 1981 to 2000 for historical simulations and 2081 to 2100 for future simulations.

Attribution methods.

We attribute the UHI intensity to contributions from different biophysical factors based on two attribution methods: the intrinsic biophysical mechanism (IBM) method (*17*) and the two-resistance mechanism (TRM) method (*18*, *19*). Both methods are based on surface energy balance equation

$$R_n = S_{in}\left(1-\alpha\right) + \varepsilon L_{in} - \varepsilon\sigma T_s^4 = H + LE + G \qquad \text{(S1)}$$

where R_n is the net surface radiation, S_{in} is the incoming shortwave radiation, L_{in} is the incoming longwave radiation, α is the surface albedo, ε is the surface emissivity, σ is the Stephan-Boltzmann constant, T_s is the land surface temperature, H is the sensible heat flux, LE is the latent heat flux, and G is the heat storage. The effect of anthropogenic heat flux is implicitly

considered in G. Sensible heat flux is parameterized using the aerodynamic resistance concept, as follows

$$H = \frac{\rho c_p}{r_a}\left(T_s - T_a\right) \qquad \text{(S2)}$$

where ρ is the air density, c_p is the specific heat of air at constant pressure, r_a is the aerodynamic resistance, and T_a is the air temperature.

a. The IBM method

In the IBM method, the latent heat flux is parameterized using the Bowen ratio (β) as

$$LE = \frac{H}{\beta} \qquad \text{(S3)}$$

Linearizing the outgoing longwave radiation term in Equation (S1) and making use of Equations (S2) and (S3), the surface energy balance equation becomes

$$S_{in}\left(1-\alpha\right) + \varepsilon L_{in} - \varepsilon\sigma T_a^4 - 4\varepsilon\sigma T_a^3\left(T_s - T_a\right) = \frac{\rho c_p}{r_a}\left(T_s - T_a\right) + \frac{\rho c_p}{r_a \beta}\left(T_s - T_a\right) + G \qquad \text{(S4)}$$

Denoting $R_n^* = S_{in}\left(1-\alpha\right) + \varepsilon L_{in} - \varepsilon\sigma T_a^4$ and $\lambda_0 = 1/\left(4\varepsilon\sigma T_a^3\right)$, one arrives at

$R_n^* = \frac{1}{\lambda_0}\left(T_s - T_a\right) + \frac{\rho c_p}{r_a}\left(T_s - T_a\right) + \frac{\rho c_p}{r_a \beta}\left(T_s - T_a\right) + G$, namely

$$T_s - T_a = \frac{\lambda_0 \left(R_n^* - G \right)}{1 + \frac{\rho c_p \lambda_0}{r_a} \left(1 + \frac{1}{\beta} \right)} \qquad \text{(S5)}$$

Further denoting $r_0 = \rho c_p \lambda_0$ and $f_{IBM} = \frac{r_0}{r_a} \left(1 + \frac{1}{\beta} \right)$ leads to

$$T_s - T_a = \frac{\lambda_0 \left(R_n^* - G \right)}{1 + f_{IBM}} \qquad \text{(S6)}$$

With the above expression for $T_s - T_a$ and assuming that the urban and rural lands share the same atmospheric properties (this assumption is consistent with the assumption made by LM3), one can express the urban-rural land surface temperature difference as

$$\Delta T = \left(\frac{\partial T_s}{\partial R_n^*} \right)^{IBM} \Delta R_n^* + \left(\frac{\partial T_s}{\partial r_a} \right)^{IBM} \Delta r_a + \left(\frac{\partial T_s}{\partial \beta} \right)^{IBM} \Delta \beta + \left(\frac{\partial T_s}{\partial G} \right)^{IBM} \Delta G \qquad \text{(S7)}$$

Where

$$\left(\frac{\partial T_s}{\partial R_n^*} \right)^{IBM} = - \left(\frac{\partial T_s}{\partial G} \right)^{IBM} = \frac{\lambda_0}{1 + f_{IBM}} \qquad \text{(S8)}$$

$$\left(\frac{\partial T_s}{\partial r_a} \right)^{IBM} = - \frac{\lambda_0 \left(R_n^* - G \right)}{\left(1 + f_{IBM} \right)^2} \frac{\partial f_{IBM}}{\partial r_a} \qquad \text{(S9)}$$

$$\left(\frac{\partial T_s}{\partial \beta}\right)^{IBM} = -\frac{\lambda_0\left(R_n^* - G\right)}{\left(1+f_{IBM}\right)^2}\frac{\partial f_{IBM}}{\partial \beta} \qquad \text{(S10)}$$

$$\frac{\partial f_{IBM}}{\partial r_a} = -\frac{r_0}{r_a^2}\left(1+\frac{1}{\beta}\right) \qquad \text{(S11)}$$

$$\frac{\partial f_{IBM}}{\partial \beta} = -\frac{r_0}{r_a \beta^2} \qquad \text{(S12)}$$

The terms on the right-hand side of Equation (S7) represent contributions from net radiation, aerodynamic resistance, the Bowen ratio, and heat storage, respectively.

b. The TRM method

Different from the IBM method, the latent heat flux in the TRM method is parameterized using the aerodynamic and surface resistances (i.e., the big-leaf model)

$$LE = \frac{\rho L_v}{\left(r_a + r_s\right)}\left(q_s^*\left(T_s\right) - q_a\right) \qquad \text{(S13)}$$

where L_v is the latent heat of vaporization, r_s is the surface resistance, q_s^* is the saturated specific humidity, and q_a is the atmosphere specific humidity. Linearizing the outgoing longwave radiation and saturated specific humidity terms yields

$$S_{in}\left(1-\alpha\right)+\varepsilon L_{in}-\varepsilon\sigma T_a^4-4\varepsilon\sigma T_a^3\left(T_s-T_a\right)=\frac{\rho c_p}{r_a}\left(T_s-T_a\right)+$$
$$\frac{\rho L_v}{\left(r_a+r_s\right)}\left(q_a^*\left(T_a\right)+\frac{\partial q^*}{\partial T}\Big|_{T_a}\left(T_s-T_a\right)-q_a\right)+G \tag{S14}$$

$$T_s-T_a=\frac{R_n^*-G-\frac{\rho L_v}{\left(r_a+r_s\right)}\left(q_a^*\left(T_a\right)-q_a\right)}{\frac{1}{\lambda_0}+\frac{\rho c_p}{r_a}+\frac{\rho L_v}{\left(r_a+r_s\right)}\frac{\partial q^*}{\partial T}\Big|_{T_a}} \tag{S15}$$

Further denoting $\delta=\frac{\partial e^*}{\partial T}\Big|_{T_a}$, $\gamma=\frac{c_p P}{0.622L_v}$, and $f_{TRM}=\frac{r_0}{r_a}\left[1+\frac{\delta}{\gamma}\left(\frac{r_a}{r_a+r_s}\right)\right]$ leads to

$$T_s-T_a=\frac{\lambda_0\left[R_n^*-G-\frac{\rho L_v}{\left(r_a+r_s\right)}\left(q_a^*\left(T_a\right)-q_a\right)\right]}{1+f_{TRM}} \tag{S16}$$

Again, with the above expression for T_s-T_a and not considering changes in atmospheric properties, one arrives at

$$\Delta T=\left(\frac{\partial T_s}{\partial R_n^*}\right)^{TRM}\Delta R_n^*+\left(\frac{\partial T_s}{\partial r_a}\right)^{TRM}\Delta r_a+\left(\frac{\partial T_s}{\partial r_s}\right)^{TRM}\Delta r_s+\left(\frac{\partial T_s}{\partial G}\right)^{TRM}\Delta G \tag{S17}$$

where

$$\left(\frac{\partial T_s}{\partial R_n^*}\right)^{TRM}=-\left(\frac{\partial T_s}{\partial G}\right)^{TRM}=\frac{\lambda_0}{1+f_{TRM}} \tag{S18}$$

$$\left(\frac{\partial T_s}{\partial r_a}\right)^{TRM} = \frac{\lambda_0 \rho L_v \left(q_a^*(T_a) - q_a\right)}{\left(r_a + r_s\right)^2} \frac{1}{1 + f_{TRM}} - \left[R_n^* - G - \frac{\rho L_v \left(q_a^*(T_a) - q_a\right)}{\left(r_a + r_s\right)}\right] \frac{\lambda_0}{\left(1 + f_{TRM}\right)^2} \frac{\partial f_{TRM}}{\partial r_a} \quad \text{(S19)}$$

$$\left(\frac{\partial T_s}{\partial r_s}\right)^{TRM} = \frac{\lambda_0 \rho L_v \left(q_a^*(T_a) - q_a\right)}{\left(r_a + r_s\right)^2} \frac{1}{1 + f_{TRM}} - \left[R_n^* - G - \frac{\rho L_v \left(q_a^*(T_a) - q_a\right)}{\left(r_a + r_s\right)}\right] \frac{\lambda_0}{\left(1 + f_{TRM}\right)^2} \frac{\partial f_{TRM}}{\partial r_s} \quad \text{(S20)}$$

$$\frac{\partial f_{TRM}}{\partial r_a} = -\frac{r_0}{r_a^2}\left[1 + \frac{\delta}{\gamma}\left(\frac{r_a}{r_a + r_s}\right)^2\right] \quad \text{(S21)}$$

$$\frac{\partial f_{TRM}}{\partial r_s} = -\frac{\delta}{\gamma}\frac{r_0}{\left(r_a + r_s\right)^2} \quad \text{(S22)}$$

The terms on the right-hand side of Equation (S17) represent contributions from net radiation, aerodynamic resistance, surface resistance, and heat storage, respectively.

c. Application of the two attribution methods

In our study, the IBM and TRM methods are applied to attributing the UHI intensity of 60 cities across North America (Table S1). The required inputs of the IBM and TRM methods include sensible and latent heat fluxes, net radiation, land surface temperature, and air temperature for each land cover type. The TRM method also requires atmosphere specific humidity and air pressure. These variables are taken from the GFDL LM3 model outputs. The urban variables are the area-weighted averages of simulated results over the roof and canyon by the UCM. Hence the urban surface temperature is similar to that proposed by Ref. *32*. The rural variables are area-averages of simulated results over the natural and secondary vegetation, grassland, and pasture.

The application of the two attribution methods follows closely our recent study (*19*), which applied these two attribution methods to studying local surface temperature response to deforestation. First of all, we exclude days with precipitation and focus on the results on clear days. It should be pointed out that excluding the data on precipitating days does not mean that the resulting surface UHI will not be affected by the long-term mean precipitation. The long-term mean precipitation characterizes the local background climate and will still affect the surface temperatures (and thus the surface UHI) on clear days. We separate analyses into day and night according to the incoming shortwave radiation. When the incoming shortwave radiation is larger than 25 W m^{-2}, it is considered as daytime, otherwise it is considered as nighttime.

Acceptable agreement between the calculated ΔT and the modeled ΔT is the prerequisite for the models to correctly attribute the UHI intensity. To assess the performance of the attribution models (Equations S7 and S17) in capturing the ΔT directly inverted from the simulated outgoing longwave radiation, the root-mean-square error (RMSE) between the calculated ΔT from Equations S7 and S17 and those inverted from the simulated outgoing longwave radiation are computed. As discussed in Ref. *19*, with the availability of 3-hourly data, an immediate question that needs to be addressed is whether we should apply the two attribution methods at the 3-hourly scale and then aggregate the results to a longer time scale (in our case the monthly scale), or apply the methods at the monthly scale by first aggregating the input variables. We find that by aggregating the input variables to the monthly scale first and then performing the attribution, the agreement between the calculated ΔT and the modeled ΔT is better compared to performing the attribution at the 3-hourly scale and then aggregating the results to the monthly scale, which is consistent with the findings of Ref. *19*. However, the attribution results (e.g., Fig. 1) are not sensitive to this choice. As a result, we choose to aggregate the 3-hourly variables to the monthly scale where the attribution methods are applied. We exclude months if the inferred

aerodynamic and surface resistances are negative, which are about 5% and 20% of the total months for daytime and nighttime, respectively.

Despite that the attribution is performed at monthly scales, several inferred variables such as the aerodynamic and surface resistances have large uncertainties especially when the sensible or latent heat flux is very small. Additionally, neglecting higher-order terms in the Taylor series expansion (Equations S7 and S17) can also introduce large errors when the perturbations are large (*19*). To further improve the accuracy of the models, we adopt two strategies to reduce the RMSE of the IBM and TRM methods (*19*). First, we exclude months if the absolute values of monthly sensible and latent heat fluxes are less than 15 W m^{-2} in the daytime and 5 W m^{-2} at night. The criterion is reduced at night in order to retain as many data points as possible for attribution. Second, we introduce a weighted approach to calculate the partial derivatives in the equations S7 and S17 based on urban and rural variables, as follows

$$Y = \frac{Y_{rural} + mY_{urban}}{1+m} \qquad \text{(S23)}$$

where Y is the final partial derivative used in the model, m is average weight, Y_{rural} and Y_{urban} are the partial derivatives calculated only using rural or urban variables, respectively.

The introduction of *m* is to account for the effects of neglected higher-order terms in the Taylor series expansion, which can be important when the urban-rural differences (represented by Δ) are not sufficiently small. The value of *m* is optimized by minimizing the RMSE (Table S2). We find that while the *m* value strongly affects the RMSE, it does not affect our findings about the attribution qualitatively. For example, when *m* = 1 which gives equal weights to urban and rural sensitivities is used, the daytime attribution indicates that the surface resistance contributes mostly to the surface UHI, which is similar to the finding from Fig. 1b.

Because of the criteria imposed for the attribution, some cities do not pass the criteria, especially during nighttime (see fig. S2 where 51 cities remain). This is acceptable given our focus on the daytime UHI intensity. In addition, we make sure that the cities in the attributions using the Sheffield forcing and GFDL forcing are the same so that the attribution results can be directly compared (fig. S2 and Fig. 1).

d. Explanation of the ΔT-precipitation covariance

Given that ΔT can be attributed to contributions from different biophysical factors, the covariance (cov) between ΔT and precipitation (P) can be also explained by the covariance between different contributions and P, which for the IBM and TRM methods are as follows

$$\begin{aligned}\mathrm{cov}\left(\Delta T_s^{IBM}, P\right) = &\mathrm{cov}\left(\left(\frac{\partial T_s}{\partial R_n^*}\right)^{IBM} \Delta R_n^*, P\right) + \mathrm{cov}\left(\left(\frac{\partial T_s}{\partial r_a}\right)^{IBM} \Delta r_a, P\right) + \\ &\mathrm{cov}\left(\left(\frac{\partial T_s}{\partial \beta}\right)^{IBM} \Delta \beta, P\right) + \mathrm{cov}\left(\left(\frac{\partial T_s}{\partial G}\right)^{IBM} \Delta G, P\right)\end{aligned} \tag{S24}$$

$$\begin{aligned}\mathrm{cov}\left(\Delta T_s^{TRM}, P\right) = &\mathrm{cov}\left(\left(\frac{\partial T_s}{\partial R_n^*}\right)^{TRM} \Delta R_n^*, P\right) + \mathrm{cov}\left(\left(\frac{\partial T_s}{\partial r_a}\right)^{TRM} \Delta r_a, P\right) + \\ &\mathrm{cov}\left(\left(\frac{\partial T_s}{\partial r_s}\right)^{TRM} \Delta r_s, P\right) + \mathrm{cov}\left(\left(\frac{\partial T_s}{\partial G}\right)^{TRM} \Delta G, P\right)\end{aligned} \tag{S25}$$

Each term on the right-hand side can be further expressed as a fraction of the left-hand side, as shown in Fig. 2 and fig. S4.

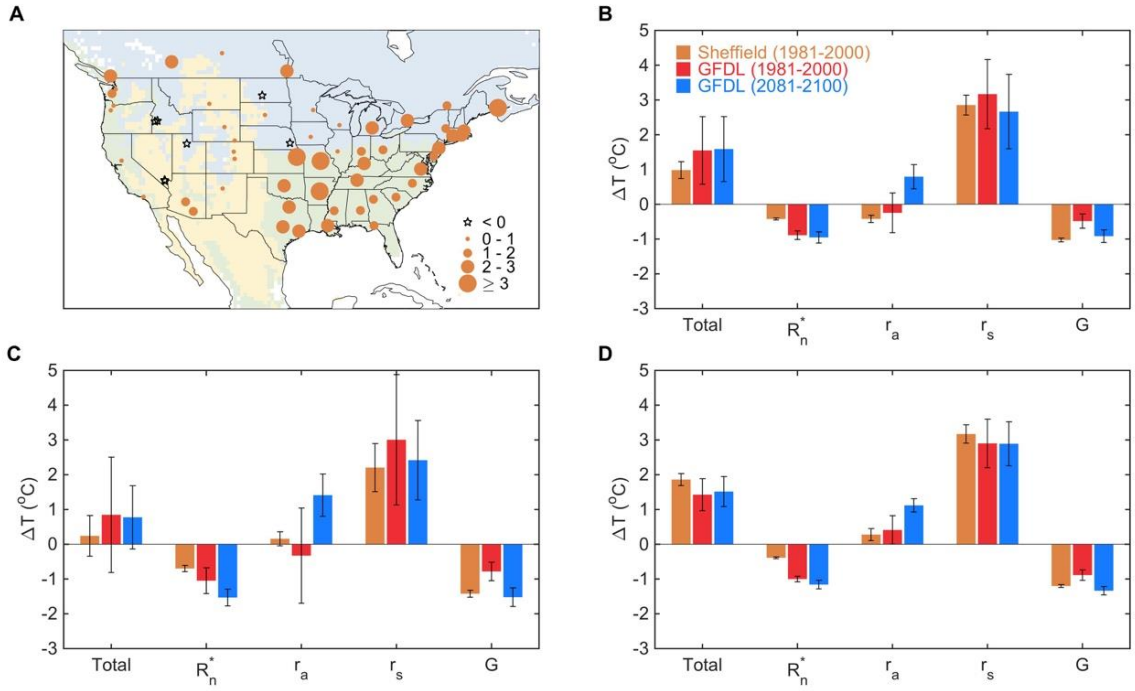

Fig. S1. Distribution and attribution of summer daytime surface UHIs across North America. Similar to Fig. 1 but the attribution is conducted for three climate zones separately (B: continental; C: arid; D: temperate).

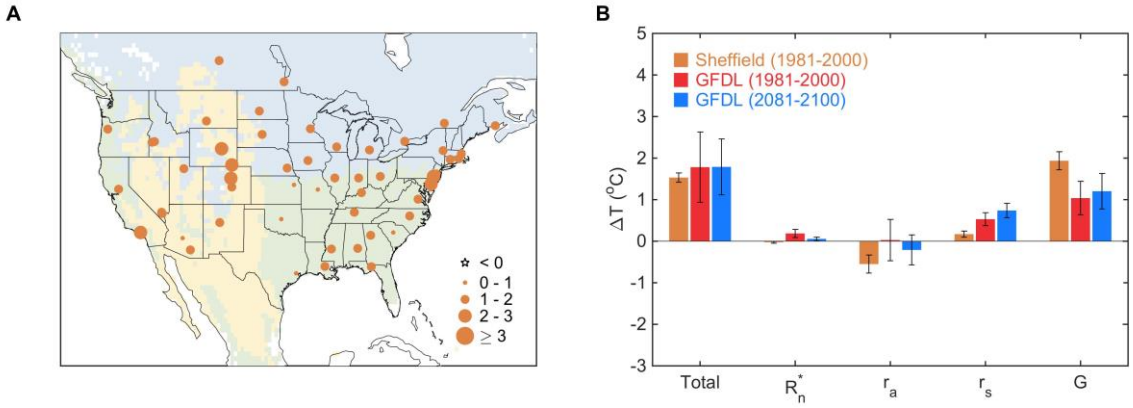

Fig. S2. Distribution and attribution of summer nighttime surface UHIs across North America. A, the distribution of simulated surface UHIs using the Sheffield forcing in 1981-2000: blue, continental region; yellow, arid region; and green, temperate region. **B**, attribution of surface UHIs in current and future climates to different biophysical factors using the TRM method. R_n^*, r_a, r_s, and G represent the contributions from net radiation, aerodynamic resistance, surface resistance, and heat storage, respectively. 'Total' represents the sum of four contributions.

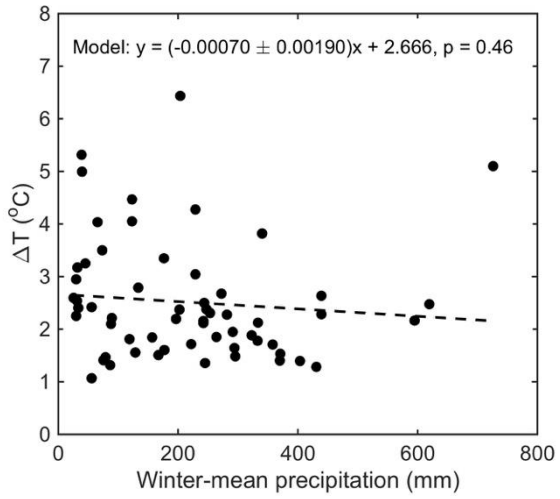

Fig. S3. Relationship between precipitation and daytime ΔT among 60 cities in winter.

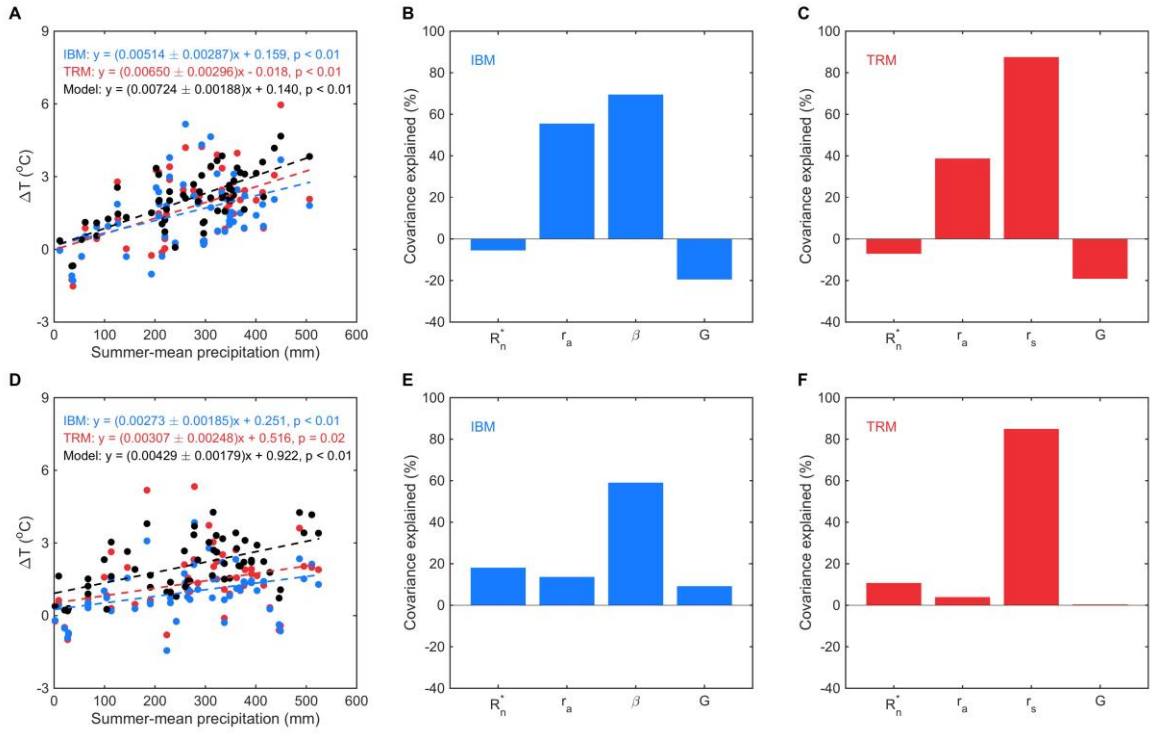

Fig. S4. Relationship between precipitation and daytime Δ*T* among cities in summer. Similar to Fig. 2 except using the GFDL forcing. The top panels are results in the historical period (1981-2000); the bottom panels are results in the period of 2081-2100 under the RCP 8.5 scenario. A, D, The correlation between daytime Δ*T* and summer-mean precipitation. Dash lines are linear regression fits to Δ*T* from the climate model (black), Δ*T* from the IBM method (blue), and Δ*T* from the TRM method (red). Parameter bounds for the regression slope are the 95% confidence interval. B, C, E, F, Δ*T*-precipitation covariance explained by contributions from radiation (R_n^*), aerodynamic resistance (r_a), the Bowen ratio (β, for the IBM method) or surface resistance (r_s, for the TRM method), and heat storage G.

Table S1. The selected cities in North America and the effective urban and rural albedo values for each city.

No.	City, State/Province	Lon	Lat	Albedo		
				Urban	Rural	Difference
1	Albany, NY	-73.75	42.65	0.237	0.196	0.042
2	Albuquerque, NM	-106.6	35.1	0.269	0.213	0.056
3	Atlanta, GA	-84.39	33.75	0.242	0.198	0.044
4	Austin, TX	-97.74	30.27	0.196	0.203	-0.007
5	Baton Rouge, LA	-91.14	30.46	0.242	0.189	0.053
6	Billings, MT	-108.54	45.77	0.256	0.195	0.061
7	Bismarck, ND	-100.78	46.81	0.249	0.208	0.041
8	Boise, ID	-116.21	43.62	0.256	0.193	0.063
9	Boston, MA	-71.06	42.35	0.237	0.192	0.046
10	Calgary, AB	-114.1	51.05	0.242	0.201	0.041
11	Casper, WY	-106.31	42.85	0.253	0.184	0.070
12	Cheyenne, WY	-104.82	41.14	0.253	0.183	0.069
13	Colorado Springs, CO	-104.82	38.83	0.269	0.188	0.082
14	Columbia, SC	-81.05	34.03	0.242	0.170	0.072
15	Columbus, OH	-82.98	39.95	0.235	0.205	0.031
16	Dallas, TX	-96.8	32.78	0.197	0.194	0.003
17	Denver, CO	-104.97	39.74	0.270	0.190	0.080
18	Des Moines, IA	-93.61	41.6	0.245	0.212	0.033
19	Dover, DE	-75.52	39.16	0.234	0.199	0.035
20	Hartford, CT	-72.68	41.76	0.237	0.191	0.047
21	Henderson, NV	-115.04	36.05	0.274	0.288	-0.013
22	Houston, TX	-95.37	29.76	0.196	0.205	-0.010
23	Indianapolis, IN	-86.16	39.77	0.236	0.207	0.029
24	Jackson, MS	-90.18	32.3	0.242	0.192	0.050
25	Jefferson City, MO	-92.17	38.57	0.199	0.200	-0.001
26	Lansing, MI	-84.55	42.73	0.237	0.199	0.039
27	Las Vegas, NV	-115.14	36.17	0.274	0.288	-0.013
28	Lincoln, NE	-96.68	40.83	0.246	0.212	0.033

29	Little Rock, AR	-92.29	34.75	0.197	0.203	-0.006
30	Los Angeles, CA	-118.24	34.05	0.270	0.217	0.053
31	Louisville, KY	-85.76	38.25	0.244	0.202	0.042
32	Madison, WI	-89.4	43.07	0.245	0.202	0.042
33	Minneapolis, MN	-93.26	44.97	0.246	0.207	0.039
34	Montgomery, AL	-86.3	32.36	0.241	0.188	0.053
35	Montreal, QC	-73.58	45.55	0.237	0.195	0.043
36	Nampa, ID	-116.57	43.54	0.257	0.215	0.042
37	Nashville, TN	-86.78	36.16	0.243	0.201	0.042
38	Oklahoma City, OK	-97.52	35.46	0.198	0.197	0.001
39	Olympia, WA	-122.9	47.04	0.261	0.198	0.063
40	Philadelphia, PA	-75.17	39.95	0.235	0.196	0.039
41	Phoenix, AZ	-112.07	33.44	0.270	0.238	0.032
42	Pierre, SD	-100.35	44.37	0.247	0.187	0.060
43	Portland, OR	-122.67	45.53	0.260	0.212	0.048
44	Providence, RI	-71.41	41.82	0.237	0.198	0.039
45	Raleigh, NC	-78.64	35.78	0.243	0.197	0.045
46	Richmond, VA	-77.43	37.54	0.244	0.192	0.052
47	Sacramento, CA	-121.48	38.6	0.273	0.216	0.056
48	Saint John, NB	-66.06	45.27	0.237	0.184	0.053
49	Salem, OR	-123.05	44.94	0.259	0.221	0.039
50	Salt Lake City, UT	-111.89	40.76	0.271	0.189	0.081
51	Saskatoon, SK	-106.67	52.13	0.242	0.207	0.035
52	Seattle, WA	-122.33	47.6	0.261	0.203	0.058
53	Springfield, IL	-89.65	39.78	0.244	0.209	0.034
54	Tallahassee, FL	-84.28	30.44	0.241	0.186	0.055
55	Topeka, KS	-95.68	39.06	0.200	0.211	-0.011
56	Toronto, ON	-79.38	43.65	0.236	0.200	0.036
57	Trenton, NJ	-74.74	40.22	0.236	0.196	0.040
58	Tucson, AZ	-110.92	32.22	0.268	0.215	0.053
59	Vancouver, BC	-123.12	49.28	0.242	0.193	0.049
60	Winnipeg, MB	-97.14	49.89	0.240	0.208	0.032

Table S2. The root mean square errors between ΔT from the climate model and those computed using the TRM method. 'Threshold' denotes the limit for the minimum absolute value of sensible and latent heat fluxes. m_{opt} is the optimal value for m. n denotes the number of valid points used to attribution.

Period		Threshold ($W\ m^{-2}$)	m_{opt}	n	RMSE (^oC)
Daytime	Sheffield (1981-2000)	15	4	2714	0.72
	GFDL (1981-2000)		6	660	1.04
	GFDL (2081-2100)		6	719	1.29
Nighttime	Sheffield (1981-2000)	5	1	630	0.46
	GFDL (1981-2000)		2	166	0.31
	GFDL (2081-2100)		2	186	0.41